

Shining Light on Missing Red Giants

Red Giant Photoevaporation in the Galactic Centre

Supervisor:
James Owen

Assessor:
Anna Penzlin

Project:
ASTR-Owen-1

CID:
01754513

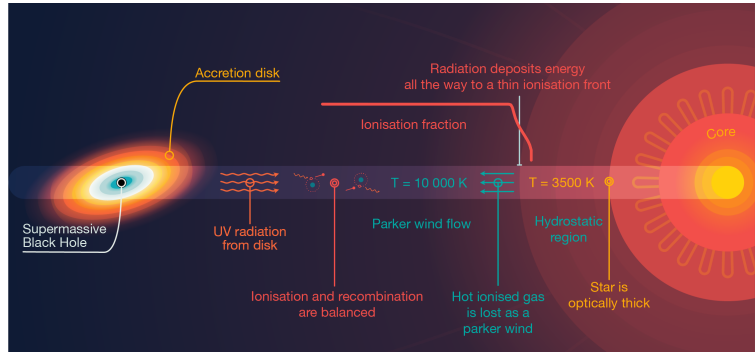
WORD COUNT: 9328

Submitted in partial fulfillment of the requirements for the MSci degree in Physics with
Theoretical Physics of Imperial College London

May 2023

When Stars Evaporate: Solving the Mystery of the Missing Red Giants

In the very heart of the Galaxy lies a supermassive black hole known as Sagittarius A*. The intense radiation emitted by the black hole can cause the outer layers of nearby stars to evaporate, much like water boiling away in a kettle. This process, known as photoevaporation, could be the key to solve the mysterious lack of red giant stars near



the galactic center. Instead of forming a dense cluster as expected, red giant stars seem to be missing from the region close to Sagittarius A*. This surprising observation contradicts theoretical models and goes against the normal behaviour of other stars. Scientists have been looking for a solution to this mystery for decades. Red giants are stars at a late stage of their life cycle. As stars like our Sun age, they expand and become cooler, eventually transforming into red giants. These enormous stars have unique properties that make them more susceptible to photoevaporation. Sagittarius A* is currently in a relatively dormant state, with its accretion disc emitting much less radiation than in the past. However, it has experienced periods of intense activity, during which it emitted copious amounts of radiation. Evidence of these past outbursts can be seen in the form of the Fermi Bubbles, two giant lobes of gas and cosmic rays extending thousands of light-years above and below the galactic plane. Photoevaporation occurs when the intense radiation from a black hole's accretion disc heats the outer layers of a nearby star. The energy from the radiation is deposited into the star's atmosphere, causing the gas to become so hot that it escapes the star's gravitational pull, evaporating into space. In my research project, I investigated the potential connection between photoevaporation and the vanishing red giants near Sagittarius A*. A crucial part of my research involved calculating the spectrum of radiation emitted by Sagittarius A*'s accretion disc. The results revealed significant emission in the ultraviolet range, which supports the possibility of photoevaporation occurring in the vicinity of the black hole during its active periods. To better understand how photoevaporation might influence the distribution of red giants, I investigated the impact of this process on their evolution. By developing a model that incorporated the effects of photoevaporation, I was able to simulate how these stars might change over time as they lose mass. A key finding of my research was the quantification of mass loss rates for red giants due to photoevaporation. I discovered that for certain sizes of red giants, the mass loss rates were significant enough to noticeably affect their evolution and distribution near the galactic center over the past 10 million years, and even completely evaporate those that got too close! My research not only enriches our understanding of the evolution of red giants in the center of our galaxy, but also sheds light on the broader implications of photoevaporation in other active galactic centres. The mystery of missing red giants is an intriguing challenge for astrophysicists. By examining the potential influence of photoevaporation, we can gain valuable insights into the complex interplay between celestial objects in the centres of galaxies.

Abstract

The observed distribution of red giant stars in the galactic centre deviates from the cusp-like arrangement predicted by theoretical and computational models. Existing explanations have thus far proven insufficient to account for this discrepancy. In this thesis, we propose a novel mechanism, wherein radiation from an accreting supermassive black hole heats the outer layers of these stars, causing them to eject mass in the form of a Parker wind. Our aim is to explore whether this photoevaporative process can offer an alternative explanation for the observed distribution of red giants in the galactic centre. We first calculate the spectrum of radiation emitted by the accretion disc and subsequently determine the ionisation fraction outside the star to find the base of the flow. With this knowledge, we apply the solutions for a steady Parker wind to find the mass loss rate. Our findings align with initial estimates and reveal that photoevaporation could have a substantial impact on the evolution of red giants near the galactic centre. We identify a specific region in our parameter space of stars that experience significant mass loss rates, which could affect their distribution over the span of 3 million years. This study presents a compelling case for further investigation of the photoevaporation hypothesis in order to ascertain its role in shaping the distribution of red giants in the galactic centre, with potential implications for the study of both the Milky Way and other galaxies.

Contents

1	Introduction	3
1.1	The Galactic Centre	3
1.2	The Problem of Missing Red Giants	3
1.3	Attempted Solutions	5
1.4	Why Photoevaporation?	6
1.5	Overview	7
2	Model and Theory	8
2.1	Accretion Theory	9
2.1.1	Eddington Limit	9
2.1.2	Accretion Disc Spectrum	10
2.2	The Stellar Wind	11
2.2.1	Hydrostatic Region	11
2.2.2	Parker Winds	12
2.3	Density Profiles	13
2.3.1	Density Profile from Steady Parker Wind	14
2.3.2	Density at Photosphere	15
2.3.3	Momentum Balance at the Interface	15
2.4	Ionisation and Recombination	16
2.5	Mass Loss Rate Estimate	17
2.6	The Star	17
2.6.1	The Core	18
2.6.2	Stellar Model	18
3	Calculations	21
3.1	Accretion Disc Spectrum	21
3.2	Ionisation Front Position	21
3.3	Mass Loss Rates	23
3.3.1	Mass Loss Rate Interpolator	24
3.4	Stellar Evolution	24
4	Results and Discussion	26
4.1	The Black Hole Spectrum	26
4.2	Mass Loss Rate Results	26
4.3	Stellar Evolution Results	28
4.4	Distance From the Black Hole	29
4.5	Implications for Other Galactic Centres	29
4.6	Other Stellar Types	30
5	Concluding Remarks	31
	Bibliography	32

1 Introduction

1.1 The Galactic Centre

The galactic centre is an area of immense interest due to its unique properties and potential insights into the formation and evolution of galaxies (Genzel et al., 2010). The central region of our Milky Way galaxy hosts a supermassive black hole with a mass of approximately 4 million times that of our Sun. This black hole, known as Sagittarius A*, or Sgr A*, is located about 26,000 light-years from Earth, making it one of the closest we can study in detail (Ghez et al., 2008).

The central region of a galaxy is where most stars are located and where the majority of the galactic mass is concentrated. The gravitational effects of this mass play a crucial role in shaping the overall structure of the galaxy, including the formation of spiral arms, the distribution of dark matter, and the formation of new stars (Dame et al., 2001). Dense molecular clouds in this region serve as nurseries for new stars, and the high-energy radiation and winds from massive stars can influence the surrounding environment and affect the evolution of nearby stars and planets.

Additionally, the region hosts a variety of exotic objects, such as pulsars, X-ray binaries, and supernova remnants, which can provide valuable insights into the physics of extreme environments and the life cycle of stars (Muno et al., 2009). Being in such close proximity, the galactic centre offers a significant opportunity to study and test the inner structure of galaxies and gain insight into how these processes affect their evolution and history.

The study of the galactic centre also provides unique opportunities to test the laws of physics under extreme conditions. The strong gravitational field in the vicinity of the black hole offers an ideal testing ground for theories such as general relativity (Amorim et al., 2019). Observations of the motion of stars around the black hole have already confirmed the predictions of general relativity to an unprecedented level of precision, further validating this fundamental theory of physics (Collaboration, 2021).

Lastly, the study of the galactic centre has important implications for astrobiology and the search for extraterrestrial life. Understanding the formation and evolution of planets in the galactic centre, as well as the environmental conditions and radiation levels that exist there, can help us better understand the potential habitability of exoplanets and the likelihood of finding extraterrestrial life.

1.2 The Problem of Missing Red Giants

The study of stellar dynamics around massive black holes has been a topic of interest in astrophysics for several decades. Peebles' seminal work (1972) found that stars around

a massive black hole are arranged in a dynamical steady state. Rather than maintaining their original orbits, two body gravitational interactions gradually push the system toward equilibrium, characterised by a stable distribution of stars. The time required to achieve this equilibrium is referred to as the relaxation time, representing the period needed for the star population to dynamically relax into the equilibrium distribution. Peebles suggested, using dimensional arguments, that the number density distribution of stars around the black hole should follow a power law with distance, forming what is now commonly called a stellar cusp.

$$n \propto r^{-\gamma} \quad (1.1)$$

Analytical proof was provided later by Bahcall & Wolf (1976) using a Fokker-Planck equation, a PDE that describes the time evolution of the probability distribution of a system (Fokker, 1914). They made several key assumptions to simplify the problem, including isotropy and that all the stars have identical masses, then solved the equation numerically, obtaining different values of γ for stars of different masses. The results of their study were further validated by other studies that used similar formalisms, such as Cohn & Kulsrud (1978) and Amaro-Seoane et al. (2004).

In addition to analytical approaches, computational efforts have been conducted to confirm the existence of stellar cusps. Shapiro & Marchant (1978) utilised Monte Carlo methods to

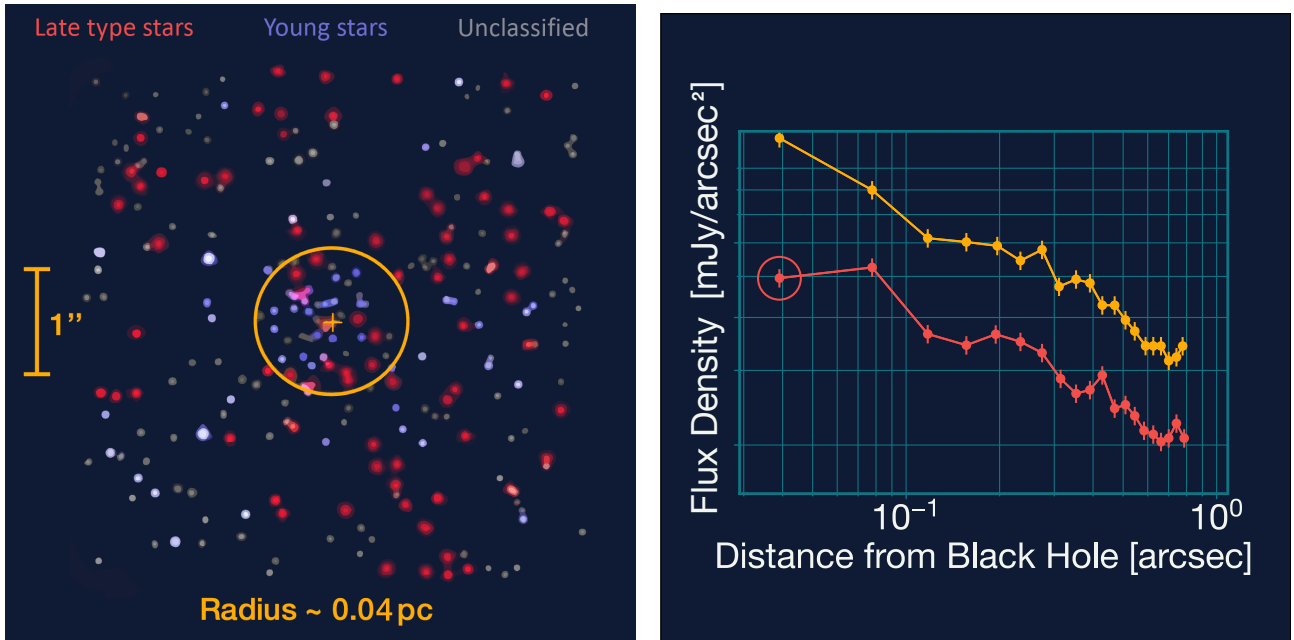


Figure 1.3: (a) Distribution of young stars (blue) and red giant stars (red), obtained from SINFONI integral field spectroscopy in the central 0.08pc of the Galaxy. The colors are based on the star's spectroscopic identification, which grey stars lack. Image adapted from Genzel et al. (2010). (b) Star surface density data from Gallego-Cano et al. (2018). The orange line shows the surface density of young stars as seen from Earth, while the red is the data for red giants. We see a surprising dip in the central region, marked by a red circle. The y values have been scaled for ease of visualisation.

simulate the behaviour of stars around a black hole. N-body simulations, free of simplifications and assumptions inherent in analytical methods, were performed by Preto et al. (2004) and Baumgardt et al. (2018).

However, Sellgren et al. (1990) observed that red giants in the Milky Way do not show a cusp distribution while studying the CO absorption line, a common indicator of giant stars. While the first observations only relied on luminosity measurements, the recent development of powerful optical instruments like the SINFONI spectrograph (Thatte et al., 1998) allowed the counting of individual stars (Bartko et al., 2010; Do et al., 2009). It is now understood that these stars, instead of forming a cusp, have a distribution that flattens as it approaches the centre (Genzel et al., 1996). This unexpected distribution has led to what is known as the “paradox of youth” in the galactic centre (Genzel et al., 2010), challenging our understanding of the dynamics of stars in this region and raising questions about the processes that may be responsible for the observed deviation from the predicted distribution.

1.3 Attempted Solutions

The search for an explanation for the missing red giants in the galactic centre has produced several proposed solutions. The phenomenon has been attributed to either the nonexistence of the stellar cusp or its hiding from observation. The former has been explained through the possibility that the cusp was either destroyed or did not have enough time to form (Merritt, 2010). Alternatively, the cusp could be composed of stellar-mass black holes or hidden because the stars closer to the centre have a lower luminosity (Löckmann et al., 2010).

Of these proposed solutions, the idea that the stellar cusp is hidden has gained more attention. Red giants, as the next evolutionary stage of solar-mass stars, are large and not very massive, with a relatively shallow gravitational potential. Coupled with their location in a very dense star cluster, this fueled the suspicion that processes could strip away the outer layer of these stars, rendering them much dimmer. Theoretical models by Genzel et al. (1996) and Dale et al. (2009) attributed this to collisions with main sequence stars and stellar-mass black holes, respectively. However, their models can only account for the central 0.01 pc of the galactic centre. In contrast, Amaro-Seoane & Chen (2014) showed how a red giant could be stripped of its atmosphere and rendered dim enough after a few transits through a star-forming disc.

Other investigations into star-disc collisions include Kieffer & Bogdanović (2016) and Amaro-Seoane et al. (2020). Kaur & Sridhar (2018) found that the gravity of an accretion disc can distort the cusp and flatten the central area, while also deforming the orbits of the stars so that they spend more time near the disc plane, thus increasing the odds of being stripped of their outer layers. Another possibility is that the gravitational forces close to the supermassive black hole could tear the atmosphere away from the red giants that get too close, a process called tidal stripping, which was proposed by Bogdanović et al. (2014).

A recent proposal by Zajaček et al. (2020a,b) attributes the loss of material to activity from Sgr A*. According to their proposal, jets coming from the supermassive black hole could remove material from the star, in a process they called jet ablation. However, as jets are very collimated, they would affect only a fraction of the stars.

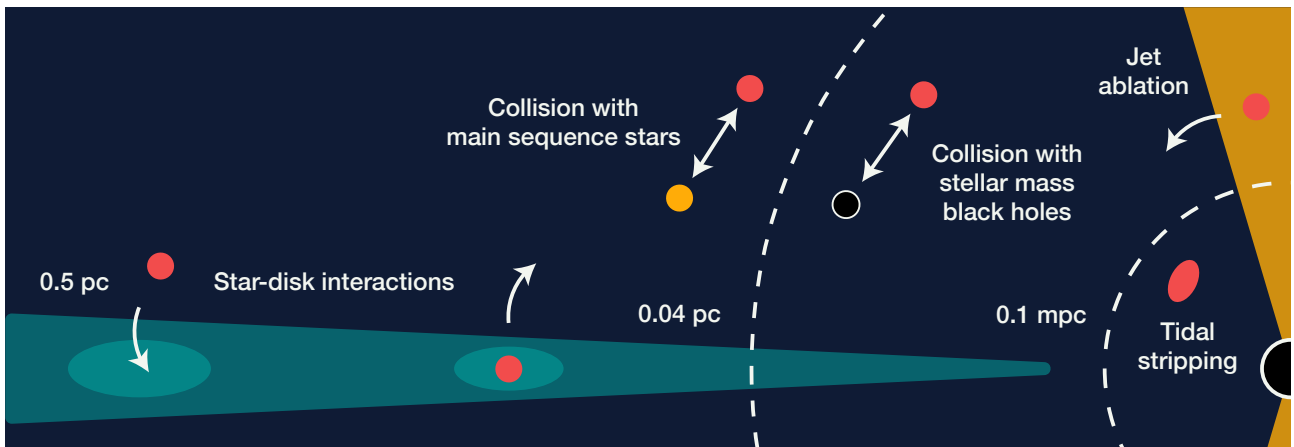


Figure 1.4: Different processes that could affect the distribution of red giants around the SMBH. Within 0.1 mpc, the gravitational forces are enough for tidal stripping to occur. Further away, jet ablation and collisions with stellar mass black holes become more relevant. Beyond 0.04 pc the main processes become collisions with main sequence stars and interactions with the stellar disc. Despite covering the whole central parsec in this way, these current known mechanisms don't add up to the total observed count of missing stars. Image adapted from Zajaček et al. (2020b).

1.4 Why Photoevaporation?

As Zajaček et al. point out, it is likely that all these processes partially contribute to the observed result. However, the current known processes fail to provide a comprehensive picture. In this vein, it is sensible to look for other processes that could contribute at other distance scales from the central black hole. Our proposal is that radiation from an accreting Sgr A* could deposit energy in the outer layers of these stars and heat them above escape temperature, leading to a loss of mass in the forms of a stellar wind. This photoevaporative process could strip the stars of their outer layers, drastically reducing their luminosity or altering their evolutionary course significantly. Unlike jets, radiation from the accretion disc is continued during the activity of the supermassive black hole, and isotropic in the plane of the galaxy, as such, it can be responsible for the lack of a larger number of stars.

Although Sgr A* is currently relatively quiescent, accreting only at $10^{-9} - 10^{-10}$ of its Eddington luminosity (Serabyn et al., 1997), there is mounting evidence that it experienced periods of increased activity in the past. Our biggest hint are the Fermi Bubbles: large-scale, gamma-ray-emitting structures extending roughly 25,000 light-years above and below the galactic plane (Su et al., 2010). These bubbles are thought to be the result of a past outburst from Sgr A* that released vast amounts of energy, driving gas and cosmic rays far away from the galactic centre (Zubovas et al., 2011). The age of the Fermi bubbles is estimated to be a few million years (Cheng et al., 2011; Guo & Mathews, 2012), suggesting that the outburst from Sgr A* occurred relatively recently in the galaxy's history.

If an event destroyed the cusp or partially stripped the stars there would not be enough time for the cusp to reform or become visible again, as the relaxation time is of the order of 1 Gyr (Zajaček et al., 2020b). Stripping could remove only the less dense atmosphere of the stars, reducing their mass by little but changing their evolutionary course considerably. With enough

atmosphere lost, the remnant can turn into a white dwarf, much less luminous and harder to observe (Deinzer & von Sengbusch, 1970). However, it is unlikely that this remnant will be disrupted by gravitational interactions and disappear completely (Lu et al., 2008).

Photoevaporative loss is known to happen to the discs of material around newly formed stars (Adams et al., 2004). Here, radiation from the star contributes to the dispersal of the disc by heating the surrounding material (Owen et al., 2012), or external radiation sources affect the disc by shaping it into a peculiar almond-like form (Johnstone et al., 1998). Photoevaporation also affects planets (Owen & Alvarez, 2016; Owen et al., 2012; Murray-Clay et al., 2009), usually large jupiter-like planets close to their star, and can change their evolutionary course considerably (Bear & Soker, 2011). It is a suspicious coincidence that, in the case of higher accretion rate from Sgr A*, Red Giants would be just the right type of star to experience this process, as their large size and low density result in a low escape temperature.

1.5 Overview

We conducted our investigation by constructing a photoevaporation model based on the recombination-limited regime described by Owen & Alvarez (2016). This choice is motivated by the large radius and low density of red giant stars, and is substantiated by the results of our calculations.

Our initial calculation involved verifying that the black hole's spectrum can drive photoevaporation in this regime. We required the radiation to ionise hydrogen and expected it to be within the extreme ultraviolet (EUV) range. This calculation also allowed us to determine the spectrum of the black hole accretion disc, which was necessary to calculate the properties of the mass loss flow.

Our primary calculation focused on evaluating the properties of mass loss by considering ionisation-recombination balance to find the position of the flow's base. Assessing mass loss is crucial because it allows us to gauge the star's immediate response to the radiation. However, it does not allow us to draw definitive conclusions about the process's relevance to the star's evolution. To understand how the star will respond to mass loss, our final calculation involved constructing a simple stellar model to estimate the adjustment of the star's radius after mass loss.

This thesis will proceed as follows: The Model and Theory section will provide a detailed outline of our model, the theoretical aspects of the relevant physical processes, and the assumptions made about the supermassive black hole, the stellar wind, and the stellar evolution. Subsequently, the Calculations section will detail the methods used for the calculations within our model, including the black hole spectrum, mass loss rate calculation, and stellar evolution adjustment. In the Discussion and Results section, we will examine the primary findings, the implications of our results for the missing giant stars problem, the limitations of our model, and potential extensions, such as the applicability of our findings to other galaxies and other star types. Finally, the Conclusion will summarise the major points of the thesis, highlighting the significance of photoevaporation in the evolution of red giant stars and the future work needed to establish testable predictions.

2 Model and Theory

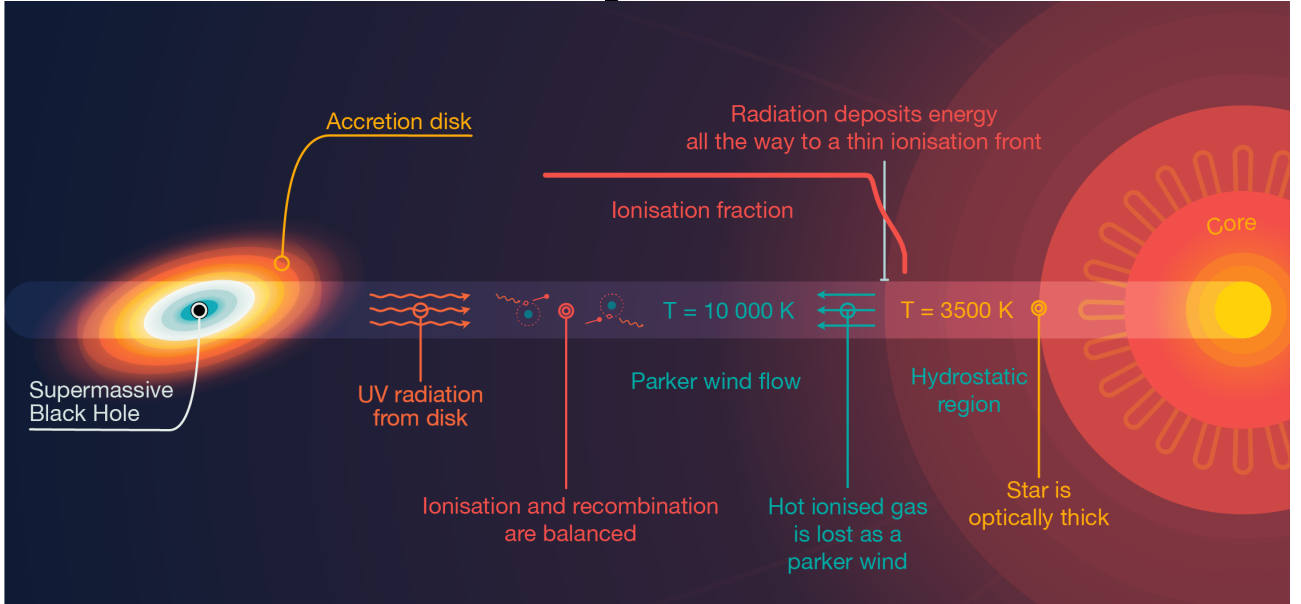


Figure 2.1: A graphic representation of our model. On the left, we have the SMBH and its accretion disk, emitting radiation. As the radiation reaches the star and the hydrogen number density increases, ionisation and recombination become relevant, dictating the morphology of the region. Here, the heated hydrogen gas is leaving the star in a flow which starts from a thin ‘ionisation front’, where the ionisation fraction rapidly decays. Beyond this, the gas is not moving and in hydrostatic equilibrium. Proceeding closer, we hit the star’s surface, where the material becomes optically thick.

In this chapter, we aim to elucidate the theoretical framework and assumptions underpinning our calculations. Our model, as depicted in the image above, is divided into three main sections, separated both physically, as they correspond to different physical regions of the model, and conceptually, as they concern different physical phenomena and different basic assumptions.

We will proceed from left to right, beginning with the supermassive black hole (SMBH) at the galactic centre. We will explore the physics of accretion and its role in generating radiation, culminating with an estimation of the disc’s emission spectrum.

Next, we will examine the region outside the star, where the radiation ionises hydrogen and deposits energy until it traverses one full optical length, at which point the material becomes optically thick to radiation. Beyond this region, radiation does not directly influence the material. Consequently, this point, which we call the ionisation front, marks a sharp drop in ionisation fraction all the way to zero and can also be regarded as the base of the flow. It is the main feature of the flow morphology, and identifying its position is necessary to calculate the mass loss rate.

Lastly, we will examine the star itself, a system delicately balanced in gravitational equilibrium that dynamically adapts to changes in its surroundings. This region is vital for comprehending the star’s response to photoevaporation and its subsequent evolution.

2.1 Accretion Theory

Accretion is the process through which black holes and other objects accumulate mass from their surroundings, typically from a gaseous disc known as an accretion disc.

For the purpose of our calculations, we adopted the thin accretion disc model, also called the Shakura-Sunyaev model (Shakura & Sunyaev, 1973). This model assumes that the disc is geometrically thin, optically thick, and in a state of Keplerian rotation, where the gas in the disc orbits the black hole at nearly the same speed as it would when only in the presence of its gravitational field. The disc's viscosity, which is attributed to turbulence, causes the gas to lose angular momentum and gradually spiral inward, allowing the material to accrete onto the black hole. As the gas spirals inwards, gravitational energy is lost through viscous interactions, and as the gas heats up it is released in the form of radiation, predominantly in the X-ray and ultraviolet bands.

As the gas falls closer, it will eventually reach the last stable orbit at roughly three times the Schwarzschild radius of the black hole (Choudhuri, 2010). This sets an inner boundary for the accretion disc, beyond which the material will plunge directly into the black hole. This innermost stable orbit (ISO) is crucial in determining the properties of the accretion disc and the energy released through the accretion process.

The radiation from the accreting gas can be associated with an effective temperature, allowing us to define a temperature profile throughout the disc, in which the material falling closer gets hotter and hotter. This effective temperature profile can be found by considering the gravitational energy lost as the material falls closer to the black hole. This energy loss results in a temperature gradient within the accretion disc, which helps us understand the disc's radiation output (Juhan Frank, 2002).

$$T_{\text{eff}}(R) = T_s \sqrt[4]{(R^{-3} - R^{-\frac{7}{2}})} \quad (2.1)$$

where

$$T_s = \sqrt[4]{\frac{GMM}{8\pi\sigma R_{\text{ISO}}^2}} \quad (2.2)$$

is the maximum temperature of the disc.

2.1.1 Eddington Limit

When a black hole or a star accretes matter, the accreting material heats up and emits radiation. As the luminosity of the object increases, the radiation pressure pushing the material outward also increases. At the Eddington limit, the radiation pressure becomes strong enough to counteract the gravitational force pulling the material inward. Consequently, the accretion process becomes self-limiting, as any further increase in the luminosity would cause the accreting material to be blown away.

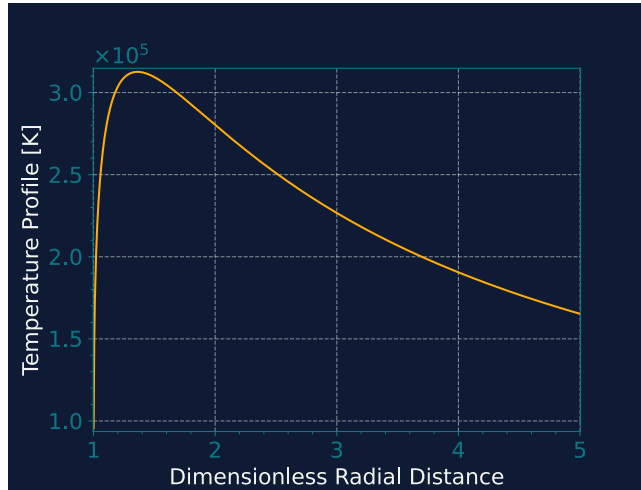


Figure 2.2: The temperature profile as a function of the dimensionless radial distance R/R_{ISO} . The temperature starts low far away from the SMBH, rising as it gets closer to peak at T_s very close to the innermost stable orbit, then rapidly drops to zero at R_{ISO} .

Mathematically, the Eddington luminosity L_{Edd} of an object of mass M can be expressed as:

$$L_{\text{Edd}} = \frac{4\pi GMcm_{\text{H}}}{\sigma_{\text{T}}} \quad (2.3)$$

where G is the gravitational constant, c is the speed of light, m_p the proton mass and σ_{T} is the Thompson scattering cross section (George B. Rybicki, 1985). The Eddington luminosity is proportional to the mass of the object, meaning that more massive objects have higher Eddington limits. In the context of accreting black holes, the Eddington limit plays an important role in determining the maximum accretion rate and luminosity that a black hole can achieve.

From this, we can find the maximum accretion rate of the SMBH. The total luminosity of the disc is dependent on the accretion rate \dot{M} (Pringle, 1981):

$$L = \frac{1}{2} \frac{GM\dot{M}}{R_{\text{ISO}}} \quad (2.4)$$

Equating 2.3 and 2.4 and solving for \dot{M} :

$$\dot{M}_{\text{Edd}} = \frac{8\pi R_{\text{ISO}} m_{\text{p}} c}{\sigma_{\text{T}}} \quad (2.5)$$

2.1.2 Accretion Disc Spectrum

The effective temperature profile allows us to determine the spectrum of radiation emitted by the accretion disc. Assuming that the disc emits as a black body, the ring elements of area $2\pi R dR$ at radius R will all have a specific luminosity given by the Planck spectrum:

$$B_{\nu}(T) = \frac{2h\nu^3}{c^2} \frac{1}{\exp \frac{h\nu}{k_{\text{B}}T} - 1} \quad (2.6)$$

where T is a function of R . This allows to set up an integral for the spectrum of the whole disc by integrating over concentric rings from the innermost stable orbit to the outer radius of the disc:

$$L_\nu = \int_{R_{\text{ISO}}}^{R_{\text{out}}} 2\pi^2 R B_\nu(T(R)) dR = 2\pi^2 R_{\text{ISO}}^2 \int_1^{r_{\text{out}}} r B_\nu(T(r)) dr \quad (2.7)$$

where we used the dimensionless variable $r = R/R_{\text{ISO}}$ and one factor of π comes from integrating over the solid angle.

This integral can be solved analytically in two limits. First for low frequencies where $h\nu \ll k_b T_s$:

$$L_\nu = 2\pi^2 R_{\text{ISO}}^2 \frac{h\nu^2}{k_b} \int_1^{r_{\text{out}}} r T(r) dr \propto \nu^2 \quad (2.8)$$

as the integral is independent of ν .

Alternatively, we can substitute $a = \frac{h\nu}{k_B T}$, which is a function of T and so of R . In this form:

$$L_\nu \propto \nu^{\frac{1}{3}} \int_{a_{\text{in}}}^{a_{\text{out}}} \frac{a^{\frac{5}{3}}}{e^a - 1} da \quad (2.9)$$

Unlike above, here the integration limits are dependent on ν , but as long as $k_B T_{\text{out}} > h\nu > k_B T_{\text{ISO}}$:

$$a_{\text{in}} = \frac{h\nu}{k_B T_{\text{ISO}}} \ll 1 \quad (2.10)$$

$$a_{\text{out}} = \frac{h\nu}{k_B T_{\text{out}}} \gg 1 \quad (2.11)$$

and the integral is roughly constant and we get $L_\nu \propto \nu^{\frac{1}{3}}$.

From these two solutions, the expected functional shape of the spectrum can be easily guessed, as it will first rise following a ν^2 dependence up until the peak contribution of the outer region of the disc, then flatten with a $\nu^{\frac{1}{3}}$ dependence, then decay rapidly as $h\nu \gg k_b T_{\text{out}}$ and the contributions to the spectrum from the highest temperature rings die off. A full solution however requires a numerical calculation, which we detail in the next chapter.

2.2 The Stellar Wind

2.2.1 Hydrostatic Region

This part of our model is characterised by two distinct regions: a radiation-driven stellar wind and a still stellar atmosphere in hydrostatic equilibrium, which the radiation doesn't reach. We consider both regions to be isothermal, although at different temperatures.

For the stellar wind region, we assume a temperature of 10^4K . This choice is motivated by the nature of the main physical processes shaping the region: ionisation and recombination. 10^4K is the temperature of the hot interstellar medium (Dalgarno & McCray, 1972), and

As we will find in our calculations, the ionisation fraction has an almost constant value of 1 up until the ionisation front, so it is reasonable to take a value of $\mu = 0.5\text{g/mol}$.

For the region outside the star instead, we chose a sample temperature of $3.5 \times 10^3\text{K}$. This is by no means the only possible temperature, but it is a temperature in a reasonable range for a red giant, and sets the order of magnitude for the calculation. What we are expecting of our calculations is not a high precision result, but more of a qualitative estimate of the behaviour of stars under a photoevaporative process. This region is not ionised, so $\mu = 1\text{g/mol}$.

2.2.2 Parker Winds

As radiation deposits energy into the gas, it will become gravitationally unbound and leave the star. In our model, we assume it does so as a Parker wind, as this requires very minimal assumptions:

- i The gas is moving radially outwards
- ii The gas is in the presence of a gravitational field
- iii The wind has reached a steady state and is time-independent

The only nontrivial assumption is the third, which is satisfied as long as the star and incoming radiation don't undergo rapid changes. This allows to write a momentum equation, with terms coming from the gravitational pressure and from the movement of the gas (Lamers & Cassinelli, 1999).

Because of mass conservation, the rate at which gas flows outwards constrains the density and velocity profile:

$$\dot{M} = 4\pi R^2 v(R) \rho(R) \quad (2.12)$$

From Newton's second law:

$$\frac{dv}{dt} = \frac{\partial v}{\partial t} + \frac{\partial v}{\partial R} \frac{\partial R}{\partial t} = v(R) \frac{\partial v}{\partial R} \quad (2.13)$$

$$v \frac{dv}{dR} + \frac{1}{\rho} \frac{dP}{dR} + \frac{GM_*}{R^2} = 0 \quad (2.14)$$

Under the assumption of a time-independent velocity profile. If the gas is ideal:

$$P = a^2 \rho \quad (2.15)$$

Where $a = \sqrt{\frac{RT}{\mu}}$ is the speed of sound. Which allows to rewrite the pressure gradient term as:

$$\frac{1}{\rho} \frac{dP}{dR} = \frac{a^2}{\rho} \frac{d\rho}{dR} \quad (2.16)$$

The term $\frac{1}{\rho} \frac{d\rho}{dR}$ can be rewritten using mass conservation:

$$\frac{1}{\rho} \frac{d\rho}{dR} = -\frac{2}{R} - \frac{1}{v} \frac{dv}{dR} \quad (2.17)$$

Plugging in, the momentum equation becomes

$$v \frac{dv}{dR} + a^2 \left\{ -\frac{1}{v} \frac{dv}{dR} - \frac{2}{R} \right\} + \frac{GM_*}{R^2} = 0 \quad (2.18)$$

We note that the first two terms can be rewritten as $\frac{1}{2} \frac{d(v^2)}{dR}$ and $-\frac{d \log v}{dR}$. Integrating and fixing the constant by requiring We can solve for the mach number using the Lambert W function, defined as the inverse of $f(x) = xe^x$. The function has two branches and the correct one has to be chosen to obtain the correct physical solution.

Where the critical radius R_c is:

$$R_c = \frac{GM_*}{2a^2} \quad (2.19)$$

$$\mathcal{M}(R) = \sqrt{-W_k \left[-\frac{R_c^4}{R^4} e^{3-4\frac{R_c}{R}} \right]} \quad (2.20)$$

Here, $k = 0$ for $R < R_c$ and $k = -1$ for $R > R_c$.

As the argument of W_k is negative, we need to ensure we choose the correct branch of the W function to have a smooth increasing solution. For $R < R_c$, we use the main branch W_0 , while for $R > R_c$, we use the W_{-1} branch. This choice ensures that the solution is consistent with mass conservation, as it will be ascending for $R > R_c$.

2.3 Density Profiles

In the region behind the ionisation front, the gas will have a zero rms velocity, and we will assume it to be still and in hydrostatic equilibrium. Under these conditions, the momentum equation is simpler:

$$\frac{1}{\rho} \frac{dP}{dR} + \frac{GM_*}{R^2} = 0 \quad (2.21)$$

And it can be solved to give the hydrostatic density profile.

$$\rho(R) = \rho_s e^{2\frac{R_c}{R} - 2\frac{R_c}{R_s}} \quad (2.22)$$

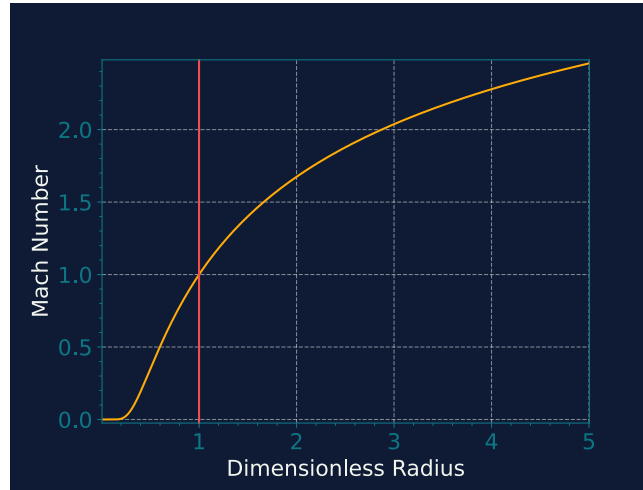


Figure 2.3: The mach number of a Parker wind, as a function of the dimensionless radial distance R/R_c . The red vertical line marks the critical radius, which in the steady parker wind coincides with the sonic point, the point at which the flow velocity rises above the sound speed.

with

$$R_c = \frac{GM_*\mu}{2RT} = \frac{GM_*}{2c_s^2} \quad (2.23)$$

G gravitational constant, M_* Mass of the star, R ideal gas constant, T Temperature (constant), r_c Parker wind critical radius, R_s radius of the star (at the photosphere), and c_s is the speed of sound.

For the Parker wind region instead, the density profile is given from mass conservation and the Parker wind velocity. Since the total mass flowing outwards has to be the same at all distances:

$$\dot{M} = 4\pi R^2 \rho(R) v(R) \quad (2.24)$$

Which allows to find the density profile by solving for ρ :

2.3.1 Density Profile from Steady Parker Wind

Using mass conservation $\dot{M} = 4\pi R^2 \rho(R) v(R)$

obtain $R^2 \rho(R) v(R) = R_c^2 \rho(R_c) v(R_c)$

recall $v(R_c) = c_s$ so:

$$\rho(R) = \frac{R_c^2}{R^2} \frac{\rho(R_c)}{\mathcal{M}(R)} \quad (2.25)$$

If the density at some other radius, say the ionisation front R_{IF} , is known, then:

$$\rho(R_I) = \frac{R_c^2}{R_{\text{IF}}^2} \frac{\rho(R_c)}{\mathcal{M}(R_{\text{IF}})} \quad (2.26)$$

so we can rewrite:

$$\rho(R) = \frac{R_{\text{IF}}^2}{r^2} \frac{\mathcal{M}(R_{\text{IF}})}{\mathcal{M}(R)} \rho(R_{\text{IF}}) \quad (2.27)$$

2.3.2 Density at Photosphere

The knowledge that the region outside the star is hydrostatic and the value of the density at a single radial distance are sufficient to find the full density profile of the region. We assume the radius of a star is defined as the radius at which the star becomes opaque. We can find the density at the surface by demanding that the optical depth is of order unity at the depth of one hydrostatic scale height.

$$\rho_s \kappa H = 1 \quad (2.28)$$

Where κ is opacity in cm^2/g and H is scale height:

$$H = \frac{\mathcal{R}T}{\mu} \frac{R^2}{GM_*} \quad (2.29)$$

2.3.3 Momentum Balance at the Interface

In our approximation of a point-like ionisation front, we have a discontinuous interface between the two regions, the Parker wind region and the hydrostatic region. In these regions, the gas has very different states. On one side, the gas is moving, while on the other it is not. Although we assume both to be isothermal, we also assumed very different temperatures for the two regions. There is no reason then for the gas on the two sides of the interface to have the same pressure or density. To be consistent with our steady state assumption, we have to impose a momentum balance condition, so that the force on one side of the interface balances out the force on the other side.

Because of momentum conservation, we can relate the pressure and velocity on both sides of the interface:

$$\rho_p v^2 + P_p = P_h \quad (2.30)$$

Where P_p and P_h are the pressures in the Parker wind and hydrostatic region respectively. Since the gas is ideal, we can substitute Equation 2.42 on both sides, then solve to get:

$$\rho_p = (1 + M^2(R_{\text{IF}}))^{-1} \frac{T_h}{T_p} \rho_h \quad (2.31)$$

2.4 Ionisation and Recombination

The position of the base of the flow depends on how deep the radiation can penetrate these outer layers. For stars such as red giants, this is controlled by ionisation and recombination in the stellar wind region.

We assume that the radiation from the SMBH will be able to ionise hydrogen, and that metallicity will be low enough to be irrelevant. The ionisation rate is $n_H\Gamma$, with:

$$\Gamma = \int_{13.6\text{eV}}^{\infty} \frac{L_\nu e^{-\tau_\nu}}{h\nu} \frac{\sigma_\nu}{4\pi d^2} d\nu \quad (2.32)$$

Where σ_ν is the photoionisation cross-section, n_H Hydrogen number density, $\tau_\nu = \int n_{H1}\sigma_\nu dr$ is the optical depth, d distance from radiation source and $\frac{L_\nu}{h\nu}$ is the photon flux per frequency in the interval $[\nu, \nu + d\nu]$. The integral starts from 13.6 eV, the energy of the hydrogen ground state, as this is the lowest energy an ionising photon can have.

The recombination rate instead is $n_e n_p \alpha_B$ where n_H , n_e , n_p are the Hydrogen, electron and proton number densities and α is the recombination coefficient. Assuming the recombination time is faster than the flow timescale, the gas can be considered to be in local equilibrium, and the amount of ionised gas is controlled by the balance of ionisation and recombination.

$$n_H\Gamma = n_e n_p \alpha_B \quad (2.33)$$

It is convenient to define the ionisation fraction $X = \frac{n_e}{n_H}$, which allows to write the number density of non-ionised hydrogen as $n_{HI} = (1 - X)n_H$.

We note that non-ionised hydrogen contributes to the ionisation rate, while the proton and electrons contribute to the recombination rate. Then ionisation-recombination balance becomes:

$$(1 - X)n_H\Gamma = X^2 n_H^2 \alpha_B \quad (2.34)$$

with the assumption that the gas is neutrally charged ($n_p = n_e = n_H X$). At fixed distance from a star Γ , n_H and α_B are constant and we can solve for X :

$$X = \frac{-\Gamma \pm \sqrt{\Gamma^2 + 4n_H \alpha_B \Gamma}}{2n_H \alpha_B} \quad (2.35)$$

Where only the positive solution is physical.

From this result, some initial considerations can be made: throughout the region, we expect the ionisation fraction to drop as the optical depth τ_ν increases, resulting in a lower Γ . As we will see later, this change is rather abrupt, creating a thin region in which the ionisation fraction rapidly drops to zero. This region is what we call ionisation front. It is not a point-like region, but its extension in this situation is small enough that for all purposes it can be considered a single point. Our calculations will mainly revolve in figuring out the radial position of the ionisation front, as this is what we will consider as the base of the flow.

2.5 Mass Loss Rate Estimate

If we're willing to make some crude assumptions, we can get an analytical estimate of the mass loss rate (Owen & Alvarez, 2016). First, we estimate the density at the flow base n_b by imposing that all the radiation from the incoming flux is absorbed over one scale height (which for a Parker wind is set by R_c):

$$\mathcal{F} = \int_{R_s}^{\infty} \alpha_B X n_H^2 dR \approx \alpha_B n_b^2 R_c \quad (2.36)$$

which gives:

$$n_b = \sqrt{\frac{\mathcal{F}}{\alpha_b R_c}} \quad (2.37)$$

by assuming the base of the flow is at the star's radius, we have all the information required to find the mass loss rate from Equation 2.12:

$$\dot{M} = 4\pi R_s^2 c_s \mathcal{M}(R_s) m_H n_b \quad (2.38)$$

2.6 The Star

Red giant stars are an important phase in the life cycle of low to intermediate-mass stars (0.3 to $8M_\odot$) and constitute a significant fraction of the stellar population in the Universe. These stars are characterized by their large radii (0.5 to 2AU) and their relatively cool surface temperatures, typically between 3,000 and 4,000K (Schwarzschild & Härm, 1958). This combination of size and temperature gives them their distinct red appearance and the name "red giant."

The evolution of a star into a red giant begins when its core hydrogen supply has been exhausted, and the star can no longer maintain nuclear fusion through the proton-proton chain. Consequently, the core contracts and heats up, triggering hydrogen shell burning around the inert helium core (Iben, 1965). This process increases the star's luminosity, causing the outer layers to expand and cool, giving rise to the typical red giant characteristics (Kippenhahn & Weigert, 1990).

Red giant stars can be further classified into two distinct groups: red giant branch (RGB) stars and asymptotic giant branch (AGB) stars. While both types of red giants undergo similar processes, the primary difference lies in the stage of nuclear burning occurring in the core. In RGB stars, the core is primarily composed of inert helium, and nuclear fusion is limited to hydrogen shell burning around the core. On the other hand, AGB stars have already experienced a helium flash, igniting helium burning in the core and resulting in the production of carbon and oxygen. This advanced stage of core burning in AGB stars leads to a more complex structure, with both hydrogen and helium shell burning surrounding the core Iben &

Renzini (1983). In our model, we will focus on RGB stars, as their simpler internal structure is more suited for our analysis.

2.6.1 The Core

Degenerate compact objects, such as the cores of red giant stars, have a unique relationship between their mass and radius due to the degenerate nature of the matter within them. In these objects, the pressure supporting them against gravitational collapse is primarily provided by the degenerate electrons, which obey the Pauli exclusion principle (Chandrasekhar, 1931).

For degenerate objects, the mass-radius relationship can be expressed as:

$$R \propto M^{-1/3}$$

This relationship indicates that as the mass of a degenerate object increases, its radius decreases. This is contrary to what one would expect for non-degenerate objects, where an increase in mass generally leads to an increase in size. The negative correlation between mass and radius in degenerate objects is a result of the increased degeneracy pressure provided by the electrons as the object becomes more compact.

2.6.2 Stellar Model

Since our calculations provide the mass loss rate of the star, our stellar model will be necessary to find how the star evolves under mass loss from its outer layers. We would like to be able to know how the star's radius adjusts after losing a certain amount of mass. During this process we assume that the star adjusts adiabatically, as the mass loss happens on timescales much longer than the one set by the speed of sound and radius of the star. By assuming that the core doesn't change, i.e. the process is taking place on timescales shorter than the star's evolutionary timescale, we can use the core mass as a constant of our model. Then, the physical processes governing the stellar structure and the future mass of the star will be restrictive enough to determine the future radius.

The temperature at the surface of the core is dictated by the hydrogen burning temperature for the p-p cycle, which is about 4×10^7 K.

We assume that the hydrostatic region is adiabatic as it is governed by convection. Convection occurs when the temperature gradient in a fluid becomes steeper than the adiabatic gradient, which leads to an efficient transport of heat through the fluid. In this case, the temperature gradient remains close to adiabatic because convection rapidly redistributes heat, preventing significant deviations from the adiabatic gradient (Kippenhahn & Weigert, 1990).

The gas is adiabatic

$$P = K\rho^\gamma \quad (2.39)$$

and hydrostatic

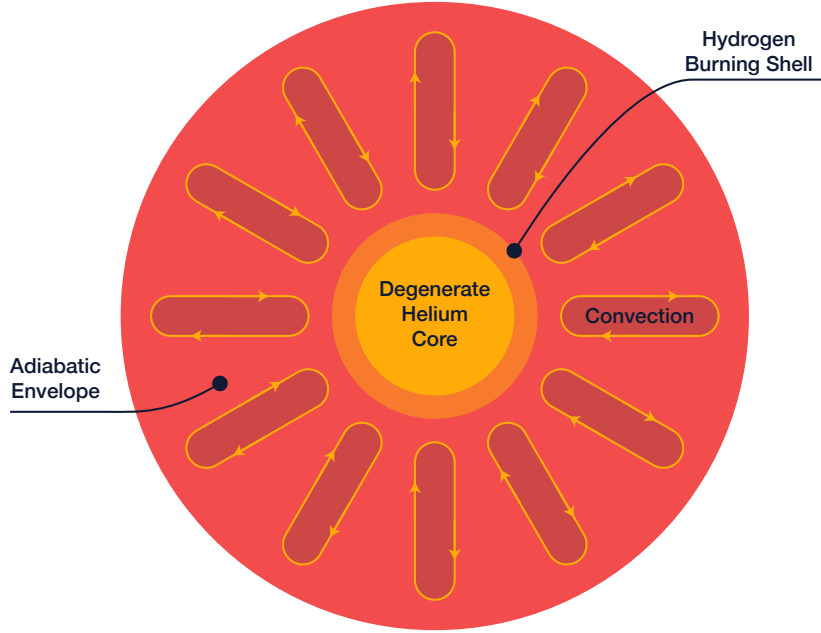


Figure 2.4: A schematic of our model. Following the structure of a RGB red giant, our model assumes a helium core supported by degeneracy pressure, surrounded by a shell of burning hydrogen, which is then surrounded by an envelope of hydrogen gas. Here, convective motion keeps the gas adiabatic.

$$\frac{dP}{dR} = -\frac{Gm}{R^2}\rho \quad (2.40)$$

where m is the mass contained in the volume of the star of radius $< R$.

Differentiating 2.39 and substituting 2.40 we obtain an equation for the density gradient:

$$\frac{d\rho}{dR} = -\frac{1}{K\gamma} \frac{Gm}{R^2} \rho^{2-\gamma} \quad (2.41)$$

To find the temperature gradient, we differentiate the ideal gas law:

$$P = \frac{\mathcal{R}T}{\mu}\rho \quad (2.42)$$

$$\frac{dT}{dR} = \frac{\mu}{\mathcal{R}} \left\{ \frac{1}{\rho} \frac{dP}{dR} - \frac{P}{\rho^2} \frac{d\rho}{dR} \right\} \quad (2.43)$$

substituting 2.40 and 2.41, and noticing that $\rho^{-\gamma}P = K$, we obtain:

$$\frac{dT}{dR} = \frac{1-\gamma}{\gamma} \frac{\mu}{\mathcal{R}} \frac{Gm}{R^2} \quad (2.44)$$

3 Calculations

3.1 Accretion Disc Spectrum

To numerically evaluate the spectrum of the accretion disc, we used the trapezoid integration routine from the `scipy.integrate` Python module. For each value of the frequency ν , we numerically integrated the integrand in equation 2.7, using 300 logarithmically spaced bins. As integration variable we used the dimensionless radius $r = \frac{R}{R_{\text{ISO}}}$. We used an integration range starting from $1 + 10^{-5}$ (to avoid numerical rounding errors) all the way to the value of 10^4 . Values further out bring virtually no contribution to the integral as the temperature is too low.

It is also important to note that the integral has two physical cutoffs. One is the distance at which the temperature of the disc reaches the temperature of the surrounding interstellar medium. The other is of the distance at which the ring simply ceases to be. We found that choosing values beyond 10^4 did not significantly impact our result.

In the frequency range, we limit our calculation to the range $(10^{-5}, 10^5)$. The frequency range we are truly interested is the EUV, which includes radiation from 13.6eV to a couple thousands of eV, as this is radiation capable of ionising hydrogen and depositing sufficient energy in the star's surroundings. However, we choose a larger range for testing purposes.

3.2 Ionisation Front Position

To fulfil our aim of calculating the photoevaporative mass loss rate, we want to be able to find the density and velocity at a known position. An obvious candidate for such position is the base of the flow, which in our model is located at the ionisation front. Hence, we want to be able, given the incoming flux, the mass and radius of the star, to find where the ionisation front is located. This is the aim of this calculation.

There are several variables affecting the black hole flux and spectrum, but we wish to evaluate our model on a grid over some parameter space, and having multiple parameters for a single physical aspect of the calculation is inconvenient. For this reason, we chose to vary only the accretion rate of the SMBH, expressed in fractions of the Eddington rate. While this doesn't seem to encompass all the possible spectra, which will also depend on black hole mass (fixed if we only consider Sgr A*) and on the distance from the SMBH, we see that the radiation flux only appears in the calculation of Γ , where it is divided by d^2 . Since the number of ionising photons is directly proportional to the accretion rate, the value L_ν/d^2 can be controlled by a single parameter. Thus our parameter space will be three dimensional, composed of the star's radius at the photosphere R_s , the star's mass M_* and the accretion rate of the SMBH, expressed as a dimensionless fraction of the Eddington rate $\dot{m} = \frac{\dot{M}}{M_{\text{Edd}}}$. The distance will be fixed at a value of $d = 0.05\text{pc}$

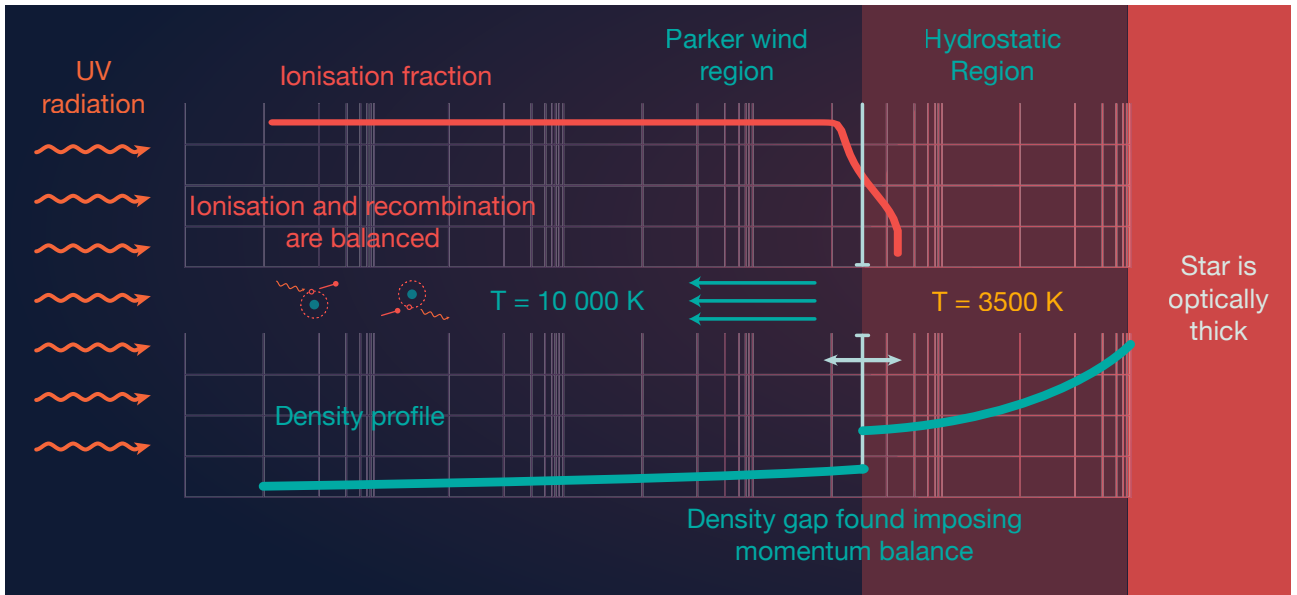


Figure 3.1: A schematic representing our calculation of the ionisation front position. We start by guessing the position, then calculate the density profile in the hydrostatic region and find the density in the Parker wind region by imposing momentum balance at the interface. From here, we can calculate the ionisation front position and compare it to our guess.

To find the position of the ionisation front, we apply the shooting method: we first guess its position, calculate the density profile based on this guess and use it to integrate inwards and determine where the ionisation fraction falls to 0. However, this position will not coincide with our guess. To fix this boundary condition we defined a function that takes our guess as an input and calculates how far the calculated IF falls from the guess. Then, we solve for a zero of this function using the `scipy.optimize.brentq` solver.

We work in dimensionless radial units $r = R/R_c$, to avoid dealing with large numerical values and carrying around the units, while also allowing to scale the algorithm depending on the position of the critical radius. Starting from our guess, we choose a position far enough from the star that the optical depth already traversed by the radiation is negligible. Then, we numerically integrate inwards finding the value of X and Γ at each step. We proceed this way until, ideally, $X = 0$. However, as the numerical value will never be exactly 0, we chose an arbitrarily low value of $X < 10^{-4}$, which was deemed acceptable as choosing a lower one wouldn't affect the result. We then calculate the difference between the guessed position of r_{IF} and the result.

Here is a break down of the steps we followed. The radial steps are spaced logarithmically starting from $r_0 = 10$, so they get smaller the closer to the star.

- i. Divide radially into log-spaced bins $[r^0, \dots, r^i, \dots r^n]$
- ii. Initialise with $X^0 = 1$, $\tau_\nu^0 = 0$
- iii. Evaluate Γ^0
- iv. Determine X^1 by applying ionisation-recombination balance

- v. Calculate $\tau_\nu^{i+1} = \tau_\nu^i + n_H \sigma_{\nu_0} (1 - X^i) (r^{i+1} - r^i)$, $\Gamma^{i+1} = \int_{13.6}^{\infty} \frac{L_\nu e^{-\tau_\nu^{i+1}}}{h\nu} \frac{\sigma_\nu}{4\pi r^2} d\nu$
- vi. Find $A^{i+1} = \frac{n_{H\alpha_B}}{\Gamma^{i+1}}$, $X^{i+1} = \frac{-1 + \sqrt{1 + 4A^{i+1}}}{2A^{i+1}}$
- vii. Repeat until X^n

To calculate X we require to know the hydrogen number density n_H . We find this by calculating the density profile $\rho(r)$ and dividing by the mass of the hydrogen atom. As we said in Section 2.3.1, the density profile is discontinuous at r_{IF} , which is where our guessed position comes into play. Our guess allows us to find the hydrostatic density profile at r_{IF} and apply momentum balance as in 2.31 to find the density on the other side of the interface. This gives a boundary condition for the Parker wind profile in 2.27, which describes the density for $r > r_{IF}$.

3.3 Mass Loss Rates

The mass loss rate can be found from 2.12 by assuming the position of the ionisation front is at the base of the flow:

$$\dot{M} = 4\pi R_{IF}^2 c_s \mathcal{M}(R_{IF}) \rho(R_{IF}) \quad (3.1)$$

We compare our mass loss rates with the analytical solution from Owen & Alvarez (2016). We expect the analytical estimate to under estimate the real mass loss rate, as it assumes the base of the flow is at the star's surface. We find that our calculation gives a value a factor of 20 larger than the analytical estimate. This number is at first glance worrying, but splitting up the product into separate terms, we see this factor emerging as a composition of the growth of the different terms in the product:

Term	Analytical Estimate	Numerical Calculation	Ratio
R_{IF}^2	0.190AU^2	0.216AU^2	1.137
$\mathcal{M}(R_{IF})$	4.71×10^{-9}	2.02×10^{-8}	4.289
$\rho(R_{IF})$	$1.24 \times 10^{-14} \text{g/cm}^3$	$4.70 \times 10^{-14} \text{g/cm}^3$	3.790
\dot{M}	$6.39 \times 10^{-16} M_\odot/\text{yr}$	$1.18 \times 10^{-15} M_\odot/\text{yr}$	18.46

Table 3.1: Comparison between the analytical solution from Owen & Alvarez (2016) and our numerical calculation, for a star of mass $M_s = 2.11 M_\odot$ and radius $R_s = 0.436 \text{AU}$, under radiation from a SMBH accreting at 1/10 of the Eddington accretion rate. The third column has the ratio of our numerical result to the analytical estimate.

This decomposition makes the large numerical difference much more understandable. The mach number and the density are the two values that contribute more to this difference, as the mach number is quite sensitive to the position of the ionisation front. In this light, a difference of a factor of 4 is acceptable.

3.3.1 Mass Loss Rate Interpolator

We ran our calculations over a grid in parameter space. To avoid unnecessary calculations, we restricted the grid by selecting masses and radii for which the escape velocity at the surface was lower than a certain value, which we determined by choosing a set of values that gave a very low mass loss rate. This also allows to have a variable grid precision which scales with the width of the explorable range.

Once we obtain the solutions over the parameter space, we interpolate them to obtain a function that can be used to rapidly obtain the mass loss rate for any point in parameter space.

3.4 Stellar Evolution

The aim of this calculation was to be able to give a qualitative statement on the evolution of the star under photo evaporative mass loss. As we decided to simulate evolution with Euler integration, we needed a model that could tell us how the star adjusted to a small mass loss at each time step.

To numerically solve the stellar model described in Section 2.6.2, we need equations 2.44 and 2.41, together with a third equation describing the change in the enclosed mass:

$$\frac{dm}{dR} = 4\pi R^2 \rho(R) \quad (3.2)$$

these have with boundary conditions at the surface $R = R_s$ and at the core $R = R_o$

We match the mass of the star:

$$m(R_s) = M_* \quad (3.3)$$

The core temperature and mass

$$T(R_o) = 4 \times 10^7 \text{K} \quad (3.4)$$

$$m(R_o) = M_o \quad (3.5)$$

At the surface, we set an arbitrarily low density, chosen so that any lower value wouldn't change the output of our model:

$$\rho(R_s) = \rho_s \quad (3.6)$$

We note that the density used in this model is completely unrelated to the surface density we used for the previous section. The physics of this model knows nothing about the opacity of the star and constraining it in that way would be too restrictive for this simple model. We assume the star to be mostly supported by radiation pressure and choose $\gamma \sim \frac{4}{3}$, minus a small numerical quantity of 10^{-12} as pure radiation pressure is unphysical.

We want our model to find a star's radius, given its mass and the mass of the core. We have to use the shooting method twice to fix two boundary conditions: the temperature at the core, and the enclosed mass at the core. The values we have to guess are the the star's radius and the temperature at the surface, which well also be the outputs of our model. We achieve this with two nested shooting methods: With a guess for the radius, we solve the problem to find the star's surface temperature by shooting inwards and integrating the model equations to find the temperature at the core. We evaluate the difference from the expected value (4×10^7) and solve for this to be 0 using the brentq solver, giving us a value of the surface temperature. Once this is done, we can calculate the enclosed mass at the core, evaluate the discrepancy from the expected one and solve again for the values that gives 0 error.

This model will output an interpolator that allows to find the star's radius for any (solvable) core mass and star mass combination.

Using a 2d root finder would require the input of a region we are certain contains the solution, which is hard to find a priori for different parameters. Instead, we nest the two problems. To find the range containing the second solution, we had to first manually evaluate our solver in a grid. This way, we determined the region in which the problem has a solution, then split it with bins of variable size to evaluate the star radii for all stars in parameter space. We interpolated these results to get a function that fit our needs.

We will keep the core mass constant during the star's evolution. This is a reasonable assumption as long as the star doesn't deviate considerably from its evolutionary course.

Once coupled with our mass loss rates, we can run a simple Euler integration to obtain the trajectory of the star in our parameter space.

4 Results and Discussion

In this section, we will recap the main findings of our investigation, discuss the implications of our results, address some limitations of our model, and explore potential applications of our findings to other galaxies and star types. Our investigation aimed to study the effect of photoevaporation on red giant stars in the vicinity of the supermassive black hole Sgr A*. We constructed a photoevaporation model based on the recombination-limited regime and carried out calculations to determine the black hole spectrum, mass loss rates, and the adjustments in stellar evolution due to mass loss.

4.1 The Black Hole Spectrum

Figure 4.1 shows the spectrum we obtained by numerical integration. This result confirms our expectations and allows us to proceed with the next calculation. The functional form of the calculated spectrum follows closely the one we expected from analytical estimates, and a large fraction of the radiation will be composed of ionising photons.

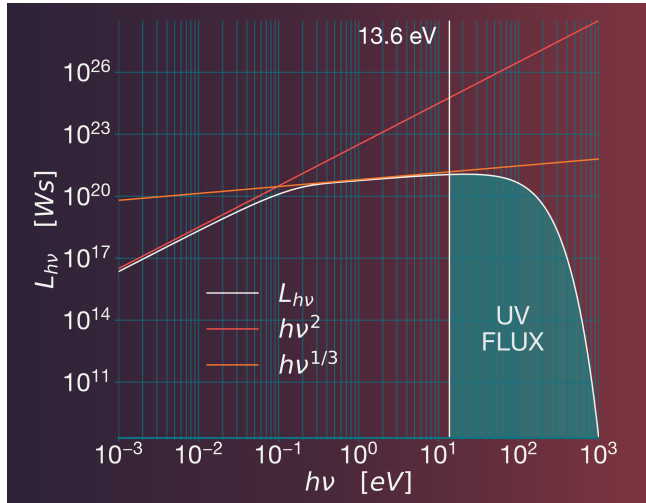


Figure 4.1: The calculated accretion disc spectrum of Sgr A*. The axes are in logarithmic scale. On the x axis we have the photon energy $h\nu$, while on the y axis we have the specific luminosity. The shaded area is the power in the EUV, of ionising photons. The red and orange straight lines are the approximate power law dependences derived in Chapter 2, shifted by an arbitrary amount for ease of visualisation.

4.2 Mass Loss Rate Results

The parameter space for this calculation was three dimensional, including the star mass M_s , the star radius R_s and the dimensionless accretion rate fraction \dot{m} . We decided to plot the mass loss rates over the $M_s \times R_s$ space, at three different values of \dot{m} : [0.1, 0.3, 1.0]

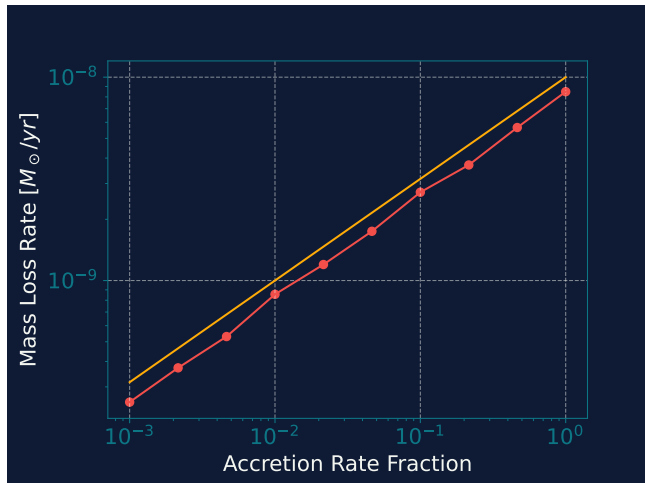


Figure 4.2: The mass loss rate scaling with \dot{m} , the fraction of the Eddington accretion rate, for a star of $1M_{\odot}$ and radius 0.5AU . In red our calculated values, while in yellow is a $\dot{m}^{1/2}$ power law. As expected, our mass loss rates scale as the square root of the flux.

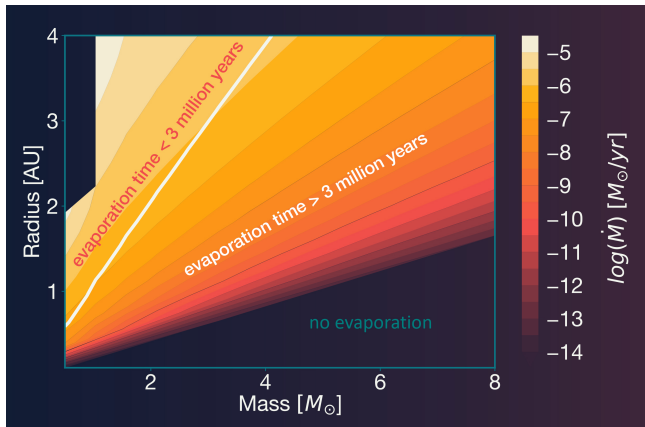


Figure 4.3: The mass loss rates for $\dot{m} = 0.3$ as a function of star radius in astronomical units and mass in solar masses. The colors represent the logarithm of the mass loss rate in M_{\odot}/yr . We see that the mass loss rates span many orders of magnitude over parameter space. The white line marks the evaporation timescale contour of 3Myr. Stars above the line take less than 3Myr to evaporate, while stars below take longer. The region marked as "no evaporation" corresponds to the section of parameter space we excluded a priori for having a large escape velocity. In the empty region in the top left corner our model failed to provide a solution, as it corresponds with a largely unphysical situation.

For better analysis, we want to convert the mass loss rates to an "evaporation timescale", that could tell us how fast the star is evaporating. If we assume constant rate, we can find this by dividing the star mass by its mass loss rate. The last activity from Sgr A* was around 10Myr, and the relaxation time of the red giant cusp is estimated at around 10^7 years. Which is why we chose 3Myr as a good timescale in which we expect stars to be significantly affected for them to go missing. As we can see from the plots, a significant fraction of the parameter space is affected, even at low accretion rate.

Our findings indicate that stars can indeed evaporate under the influence of radiation from

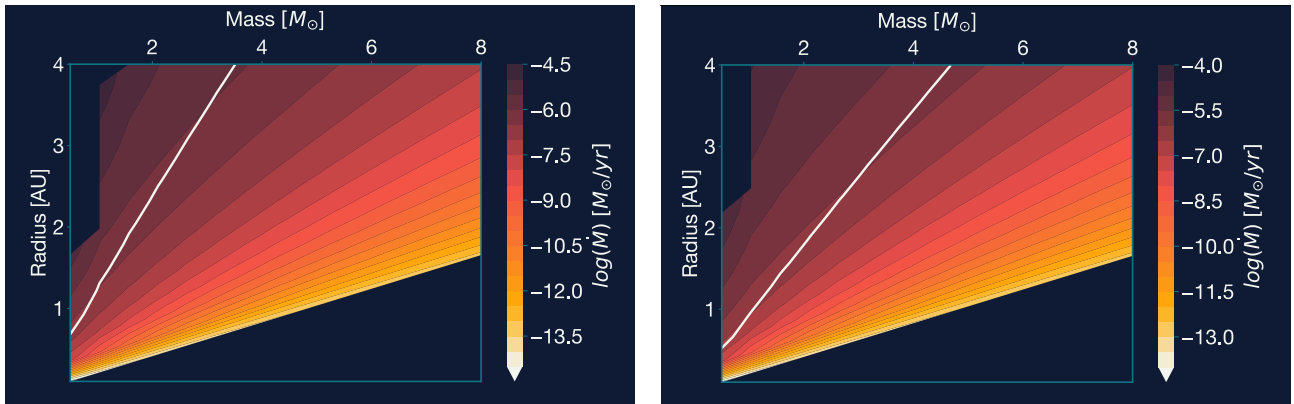


Figure 4.6: The mass loss rates for $\dot{m} = 0.1$ (a) and $\dot{m} = 1.0$ (b). We see that, as the mass loss rate scales as the square root of the flux, a large reduction in the black hole flux has only a moderate effect on the section of our parameter space that undergoes photoevaporation.

the supermassive black hole. The evaporation timescale is found to be dependent on the mass and radius of the stars, as illustrated in the plot. As expected, lighter and less dense stars are more susceptible to evaporation.

An issue that warrants further investigation is how a real red giant population is distributed in the parameter space.

A second issue with this calculation is that we do not know how a star will move in the parameter space as it loses mass. This was our reason to proceed with the next result.

4.3 Stellar Evolution Results

Figure 4.7 shows the result for our stellar evolution calculation. We let 3 different stars of the same mass but different radii evolve over the span of 3Myr.

When the stars reach a low mass, their radius seems to blow up. However at this stage other physical processes not accounted for in our model would become relevant, and the assumption of constant core mass will not hold anymore. Moreover, the non-smooth trajectory observed in the stellar evolution results can be attributed to the numerical solving method employed in certain steps, followed by interpolation. The angular jumps seen in the trajectory reflect the fact that these curves are interpolated over the grid we used to solve the problem, and could be made smoother with the use of a finer grid.

It is important to note that this model is very simple and approximate. It is only solvable in a range of core masses $[0.38, 0.42]$, which is incompatible with known sizes for red giant cores. However, its usefulness lies in the qualitative prediction it allows us to make.

Despite these limitations, our stellar evolution calculation corroborates our previous results. Before blowing up, the contours of constant core mass are roughly parallel to the contours of constant mass loss, hence the stars will experience an almost constant mass loss rate for a significant fraction of their evolution, which gives more credibility to the previous evaporation

times.

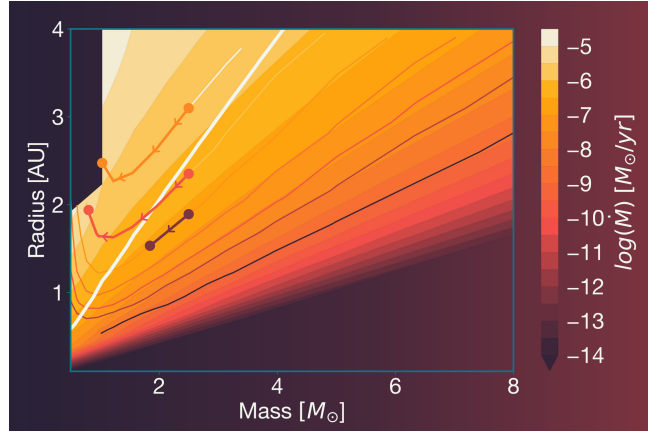


Figure 4.7: We plot the result for three stars with same starting mass but different radius, overlaid on the mass loss rate result from Figure 4.3. The colored curves represent contours of constant core mass. The direction of evolution is indicated with arrows.

4.4 Distance From the Black Hole

We carried out our calculations assuming a distance of 0.05pc from the SMBH. This was part of a choice of condensing multiple parameters of the flux in a single one, the fraction of the Eddington accretion rate, \dot{m} . Since the flux scales as $\frac{1}{d^2}$, we can adjust \dot{m} while keeping d the same to achieve any effective d : $\dot{m}_{\text{eff}} = \dot{m} \frac{d_{\text{eff}}}{d}^2$. The mass loss rate scales as the square root of the flux, so it scales as $1/d$. Hence, an increase in distance of a factor of 10, to reach 0.5pc, would decrease the mass loss rate only by a factor of 10. While this would exclude a section of the parameter space, it doesn't completely preclude the evaporation from affecting all stars. In the other case in which the star is even closer instead, the mass loss rate would increase. This feature, of linear scaling with distance allows photoevaporation to be relevant across multiple length scales, which gives it a higher chance of filling the gaps left by the other known processes that affect the distribution of red giants.

4.5 Implications for Other Galactic Centres

Our findings are applicable to other galaxies with an active SMBH. During all of our calculations, we made minimal assumptions that are dependent on the choice of galaxy. These are the mass and Eddington luminosity of the central SMBH, which could be easily modified in our code. As Eddington rate scales with mass, we expect the flux to be greater for larger supermassive black holes. As long as the spectrum remains mostly in the EUV, and doesn't move to even higher photon energies, which would require new physical processes to be investigated.

Future studies can build upon our model to investigate the role of photoevaporation in shaping the stellar population of other galactic centres, providing valuable insights into the processes governing galactic evolution.

4.6 Other Stellar Types

While our investigation focused on red giant stars, photoevaporation could also affect other star types in the vicinity of supermassive black holes. However, the details of the process could be very different than they are for red giants, as different gravitational potentials and densities would lead to a different photoevaporative regime, as mass loss rate is limited by the total power radiation can deposit in the star. Stars with deep potentials would be in the "energy-limited" regime, while small compact stars would likely be in the "photon-limited" regime described by Owen & Alvarez (2016).

Many galaxies host active SMBHs, it is clearly important to understand the implications of photoevaporation on a broader range of stars and how this process influences their evolution and fate. as this process could play an important role in shaping the environment of galactic centres.

5 Concluding Remarks

Red giant stars in the gravitational potential of the galactic centre reveal a flatter distribution than predicted by theoretical and computational models. Although some attempts to explain this have been made, a single satisfactory explanation is currently lacking. It is likely that multiple processes are contributing to this observational result, but those proposed so far fail to account for the total count of missing stars.

We investigated the new proposal that radiation from the accretion disc of a supermassive black hole can heat the outer layer of these stars above escape temperature, leading to a flow in the form of a Parker wind. To examine this possibility, we started by confirming that the UV flux from the black hole is sufficient to sustain the process. Our calculations indicated that red giants of different sizes can lose a significant portion of their mass due to photoevaporation.

Past activity from the black hole, such as accretion events, could have produced enough radiation to cause photoevaporation of nearby red giants. This led us to conclude that giant stars indeed experience photoevaporation as initially suspected. Our findings revealed that a significant portion of the parameter space will experience noticeable mass loss due to this process.

To gain a better understanding of the photoevaporation process and its implications for the observed distribution of red giants, future work could couple our model with a stellar evolution model and run simulations on a full population of stars. Projecting the results onto observables would give testable predictions in support of our hypothesis, and help establish whether this process could solve the problem of missing stars.

It is important to note that photoevaporation of stars is not only relevant in the context of the Milky Way, our closest and best example of a galaxy. We can expect this phenomenon to be present in other galaxies as well. The recent detection of an "ultramassive" black hole with a mass of 30 billion solar masses (Nightingale et al., 2023) suggests that photoevaporation could play an even more significant role in shaping the central environment of other galaxies. If many galaxies harbor ultramassive black holes with higher masses and Eddington limits, these black holes could sustain an even higher flux than Sgr A* and evaporate red giants on much shorter timescales.

In conclusion, our results suggest that photoevaporation from supermassive black holes could be a contributing factor to the missing red giants observed in the galactic centre, although multiple processes likely play a role. Our findings have implications for our understanding of galactic dynamics and could have broader applications in astrophysics. Further research is needed to refine and expand upon our model and to fully explore the extent and significance of this phenomenon. As we continue to investigate this process, we can hope to shed light on the complex interplay between supermassive black holes and the stars that populate the centres of galaxies, deepening our understanding of the intricate dance of celestial objects in the cosmos.

Acknowledgements

I would like to express my sincere gratitude to my supervisor, Dr. James Owen, for his invaluable guidance throughout the course of my research. His expertise and insights have been instrumental in shaping my work and ensuring its success. I am grateful for the time he has dedicated to helping me refine my ideas and overcome challenges.

I would also like to extend my heartfelt appreciation to my girlfriend, Fan Wang, for her constant support during this journey. Her belief in me and my abilities has been a source of motivation and strength. I am truly grateful for her presence in my life and for the happiness and balance she brings to it.

Finally, I would like to thank my family for their unwavering support and encouragement throughout my academic journey. They have consistently been by my side, motivating me to strive for excellence and achieve my full potential. I am profoundly grateful for their integral role in shaping both my personal and academic growth. Their love, guidance, and belief in me have been the foundation of my success, and I simply could not have reached this point without them.

Bibliography

- Adams, F. C., Hollenbach, D., Laughlin, G., & Gorti, U. 2004, *The Astrophysical Journal*, 611, 360, doi: 10.1086/421989 pages 7
- Amaro-Seoane, P., & Chen, X. 2014, *The Astrophysical Journal*, 781, L18, doi: 10.1088/2041-8205/781/1/L18 pages 5
- Amaro-Seoane, P., Chen, X., Schödel, R., & Casanellas, J. 2020, *Monthly Notices of the Royal Astronomical Society*, 492, 250, doi: 10.1093/mnras/stz3507 pages 5
- Amaro-Seoane, P., Freitag, M., & Spurzem, R. 2004, *Monthly Notices of the Royal Astronomical Society*, 352, 655, doi: 10.1111/j.1365-2966.2004.07956.x pages 4
- Amorim, A., Bauböck, M., Berger, J. P., et al. 2019, *Physical Review Letters*, 122, 101102, doi: 10.1103/PhysRevLett.122.101102 pages 3
- Bahcall, J. N., & Wolf, R. A. 1976, *The Astrophysical Journal*, 209, 214, doi: 10.1086/154711 pages 4
- Bartko, H., Martins, F., Trippe, S., et al. 2010, *The Astrophysical Journal*, 708, 834, doi: 10.1088/0004-637X/708/1/834 pages 5
- Baumgardt, H., Amaro-Seoane, P., & Schödel, R. 2018, *Astronomy and Astrophysics*, 609, A28, doi: 10.1051/0004-6361/201730462 pages 5
- Bear, E., & Soker, N. 2011, *Monthly Notices of the Royal Astronomical Society*, 414, 1788, doi: 10.1111/j.1365-2966.2011.18527.x pages 7
- Bogdanović, T., Cheng, R. M., & Amaro-Seoane, P. 2014, *The Astrophysical Journal*, 788, 99, doi: 10.1088/0004-637X/788/2/99 pages 5
- Chandrasekhar, S. 1931, *The Astrophysical Journal*, 74, 81, doi: 10.1086/143324 pages 18
- Cheng, K. S., Chernyshov, D. O., Dogiel, V. A., Ko, C. M., & Ip, W. H. 2011, *The Astrophysical Journal*, 731, L17, doi: 10.1088/2041-8205/731/1/L17 pages 6
- Choudhuri, A. R. 2010, *Astrophysics for Physicists* (Cambridge University Press) pages 9
- Cohn, H., & Kulsrud, R. M. 1978, *The Astrophysical Journal*, 226, 1087, doi: 10.1086/156685 pages 4
- Collaboration, G. 2021, *New Horizons in Galactic Center Astronomy and Beyond*, 528, 239 pages 3
- Dale, J. E., Davies, M. B., Church, R. P., & Freitag, M. 2009, *Monthly Notices of the Royal Astronomical Society*, 393, 1016, doi: 10.1111/j.1365-2966.2008.14254.x pages 5
- Dalgarno, A., & McCray, R. A. 1972, *Annual Review of Astronomy and Astrophysics*, 10, 375, doi: 10.1146/annurev.aa.10.090172.002111 pages 12

- Dame, T. M., Hartmann, D., & Thaddeus, P. 2001, *The Astrophysical Journal*, 547, 792, doi: 10.1086/318388 pages 3
- Deinzer, W., & von Sengbusch, K. 1970, *The Astrophysical Journal*, 160, 671, doi: 10.1086/150461 pages 7
- Do, T., Ghez, A. M., Morris, M. R., et al. 2009, *The Astrophysical Journal*, 703, 1323, doi: 10.1088/0004-637X/703/2/1323 pages 5
- Fokker, A. D. 1914, *Annalen der Physik*, 348, 810, doi: 10.1002/andp.19143480507 pages 4
- Gallego-Cano, E., Schödel, R., Dong, H., et al. 2018, *Astronomy and Astrophysics*, 609, A26, doi: 10.1051/0004-6361/201730451 pages 4
- Genzel, R., Eisenhauer, F., & Gillessen, S. 2010, *Reviews of Modern Physics*, 82, 3121, doi: 10.1103/RevModPhys.82.3121 pages 3, 4, 5
- Genzel, R., Thatte, N., Krabbe, A., Kroker, H., & Tacconi-Garman, L. E. 1996, *The Astrophysical Journal*, 472, 153, doi: 10.1086/178051 pages 5
- George B. Rybicki, A. P. L. 1985, *Radiative Processes in Astrophysics* (Wiley-VCH) pages 10
- Ghez, A. M., Salim, S., Weinberg, N. N., et al. 2008, *The Astrophysical Journal*, 689, 1044, doi: 10.1086/592738 pages 3
- Guo, F., & Mathews, W. G. 2012, *The Astrophysical Journal*, 756, 181, doi: 10.1088/0004-637X/756/2/181 pages 6
- Iben, I. 1965, *The Astrophysical Journal*, 142, 1447, doi: 10.1086/148429 pages 17
- Iben, I., & Renzini, A. 1983, *Annual Review of Astronomy and Astrophysics*, 21, 271, doi: 10.1146/annurev.aa.21.090183.001415 pages 17
- Johnstone, D., Hollenbach, D., & Bally, J. 1998, *The Astrophysical Journal*, 499, 758, doi: 10.1086/305658 pages 7
- Juhan Frank, Andrew King, D. R. 2002, *Accretion power in astrophysics*, 3rd edn., Cambridge Astrophysics S. (Cambridge University Press) pages 9
- Kaur, K., & Sridhar, S. 2018, *Monthly Notices of the Royal Astronomical Society*, 477, 112, doi: 10.1093/mnras/sty612 pages 5
- Kieffer, T. F., & Bogdanović, T. 2016, *The Astrophysical Journal*, 823, 155, doi: 10.3847/0004-637X/823/2/155 pages 5
- Kippenhahn, R., & Weigert, A. 1990, *Stellar Structure and Evolution* (Springer-Verlag Berlin Heidelberg) pages 17, 18
- Lamers, H. J. G. L. M., & Cassinelli, J. P. 1999, *Introduction to Stellar Winds* (Cambridge University Press) pages 12

- Lu, Y., Huang, Y. F., Zhang, S. N., & Lu, P. 2008, The Art of Modeling Stars in the 21st Century, 252, 343, doi: 10.1017/S1743921308023168 pages 7
- Löckmann, U., Baumgardt, H., & Kroupa, P. 2010, Monthly Notices of the Royal Astronomical Society, 402, 519, doi: 10.1111/j.1365-2966.2009.15906.x pages 5
- Merritt, D. 2010, The Astrophysical Journal, 718, 739, doi: 10.1088/0004-637X/718/2/739 pages 5
- Muno, M. P., Bauer, F. E., Baganoff, F. K., et al. 2009, The Astrophysical Journal Supplement Series, 181, 110, doi: 10.1088/0067-0049/181/1/110 pages 3
- Murray-Clay, R. A., Chiang, E. I., & Murray, N. 2009, The Astrophysical Journal, 693, 23, doi: 10.1088/0004-637X/693/1/23 pages 7
- Nightingale, J. W., Smith, R. J., He, Q., et al. 2023, arXiv e-prints, arXiv:2303.15514, doi: 10.48550/arXiv.2303.15514 pages 31
- Owen, J. E., & Alvarez, M. A. 2016, The Astrophysical Journal, 816, 34, doi: 10.3847/0004-637X/816/1/34 pages 7, 17, 23, 30
- Owen, J. E., Clarke, C. J., & Ercolano, B. 2012, Monthly Notices of the Royal Astronomical Society, 422, 1880, doi: 10.1111/j.1365-2966.2011.20337.x pages 7
- Peebles, P. J. E. 1972, The Astrophysical Journal, 178, 371, doi: 10.1086/151797 pages 3
- Preto, M., Merritt, D., & Spurzem, R. 2004, The Astrophysical Journal, 613, L109, doi: 10.1086/425139 pages 5
- Pringle, J. E. 1981, Annual Review of Astronomy and Astrophysics, 19, 137, doi: 10.1146/annurev.aa.19.090181.001033 pages 10
- Schwarzschild, M., & Härm, R. 1958, The Astrophysical Journal, 128, 348, doi: 10.1086/146548 pages 17
- Sellgren, K., McGinn, M. T., Becklin, E. E., & Hall, D. N. 1990, The Astrophysical Journal, 359, 112, doi: 10.1086/169039 pages 5
- Serabyn, E., Carlstrom, J., Lay, O., et al. 1997, The Astrophysical Journal, 490, L77, doi: 10.1086/311010 pages 6
- Shakura, N. I., & Sunyaev, R. A. 1973, Astronomy and Astrophysics, 24, 337 pages 9
- Shapiro, S. L., & Marchant, A. B. 1978, The Astrophysical Journal, 225, 603, doi: 10.1086/156521 pages 4
- Su, M., Slatyer, T. R., & Finkbeiner, D. P. 2010, The Astrophysical Journal, 724, 1044, doi: 10.1088/0004-637X/724/2/1044 pages 6
- Thatte, N. A., Tecza, M., Eisenhauer, F., et al. 1998, Adaptive Optical System Technologies, 3353, 704, doi: 10.1117/12.321638 pages 5

- Zajaček, M., Araudo, A., Karas, V., Czerny, B., & Eckart, A. 2020a, The Astrophysical Journal, 903, 140, doi: 10.3847/1538-4357/abbd94 pages 5
- Zajaček, M., Araudo, A., Karas, V., et al. 2020b, arXiv e-prints, arXiv:2011.12868, doi: 10.48550/arXiv.2011.12868 pages 5, 6
- Zubovas, K., King, A. R., & Nayakshin, S. 2011, Monthly Notices of the Royal Astronomical Society, 415, L21, doi: 10.1111/j.1745-3933.2011.01070.x pages 6